Engineered Science
DOI: https://dx.doi.org/10.30919/es8d773

Laser Induced Breakdown Spectroscopy Study of Non-Premixed Flames with Machine Learning Algorithms

Muhammad Bilal,[1, 2] Yasir Jamil[3] and Zhen-Yu Tian[1, 2,*]

Abstract

In-situ non-premixed flames were studied by the combination of laser induced breakdown spectroscopy (LIBS) and machine learning to obtain an accurate depiction of the local structures of diffusion flames. Six candles were utilized as representative sources of the non-premixed flames. The use of the intensity ratio of H/O provided the point information about the distribution of the local fuel to the oxidizer without disturbing the flame. The H/O ratio tends to decrease from the flame centerline to the border. The concentrations of H and C at the flame centerline are high due to the ionization/fragmentation of candle wax molecules. To discriminate the non-premixed flames with the candle as a representative, twenty-nine machine learning classification models of the classification learner app were implemented on LIBS data. The quadratic discriminant analysis and neural network models provided greater than 99% accuracy for training (validation) and for prediction in the case of distinguishing all candles. The cubic support vector machines (SVM) and Neural Network provided greater than 80% accuracy for both training (validation) and predicting the spatial positions in a candle flame. The reported procedure can be potentially applied to the aviation, space, and engine manufacturer industries to improve the efficiency of combustion and reduce pollutant emissions.

Keywords: LIBS; Machine learning; Non-premixed flame; Classification; Flame structure.
Received: 18 July 2022; Revised: 29 August 2022; Accepted: 10 September 2022.
Article type: Research article

1. Introduction

The non-premixed combustion has been widely used in daily life and industry. The local temperature of the flame and the flame equivalence ratio are critical parameters in the combustion of hydrocarbon fuels and have a substantial influence on the subsequent ignition but also the combustion process' uniformity. Optimizing fuel/oxidant mixing equivalency ratios is necessary for optimal combustion management and higher energy conversion efficiency. For identifying reaction processes and improving the combustion system, quantitative monitoring of the reaction concentration distribution is essential. Many scientists have focused their efforts on nonintrusive optical approaches for measuring temperature in flames. Laser-induced incandescence,[1] tunable diode laser absorption spectroscopy,[2,3] and emission-based tomography[4,5] are reliable techniques. Therefore, laser-based optical techniques for detecting combustion flow fields are crucial for monitoring and measuring the most important chemical and physical properties in combustion.[6]

Laser induced breakdown spectroscopy (LIBS) is a powerful optical emission spectroscopic technique that has attracted the interest of the scientific community because of its unique advantages and experimental simplicity for several applications.[7] It is the most rapid technique for elemental analysis, which is capable of analyzing all the elements of the periodic table in real-time from all kinds of matter (*i.e.* solid, liquid, and gaseous samples). LIBS can operate in situ, as well as remotely, providing measurements with high spatial and temporal resolution.[8,9] It is also being used for the diagnostics of the combustion process. The use of combustion is the release of alkali metals during the burning of Zhundong coal and the distribution of equivalence ratios in the flame of hydrocarbon fuels.[10-19] Machine learning (ML) is a branch of artificial intelligence that plays a significant role, ML was successfully implemented for novel thermal materials discovery,[20] ML was also used to optimize the structural parameters of the concentrated photovoltaic thermoelectric hybrid system,[21] further, its implementation in the

[1] *Institute of Engineering Thermophysics, Chinese Academy of Sciences, Beijing 100190, China.*
[2] *University of Chinese Academy of Sciences, Beijing 100049, China.*
[3] *Laser Spectroscopy Lab, Department of Physics, University of Agriculture Faisalabad, 38090, Pakistan.*
**Email:* tianzhenyu@iet.cn (ZY Tian)

combustion field is widespread.[22] Combustion regime was identified from ML trained convolutional neural networks model by Raman/Rayleigh line data.[23] Machine learning was successfully implemented on LIBS for distinction or prediction.[24-28] That is essential with the intention to control mixing processes and to avoid problems consisting of the emission of undesirable species and instabilities within the combustion process.

In this work, LIBS was used to accurately describe the local structures of certain diffusion flames in order to make a distinction among candle flames. Using the H/O intensity ratio can offer point information on the distribution of local fuel to the oxidizer without disturbing the flame. Moreover, to discriminate among candle flames twenty-nine machine learning classification models of MATLAB Classification learner app were implemented simultaneously on LIBS data.

2. Experimental section

2.1 Candle samples

Six commercially available candles named C1-C6 were utilized in this work, as shown in Fig. 1. Candle burning rates were measured to see the gross differentiation between all candles. Candles were placed on digital balance with the mass limit of 0.0001 g and noted the mass after every 60 seconds till 1200 seconds.

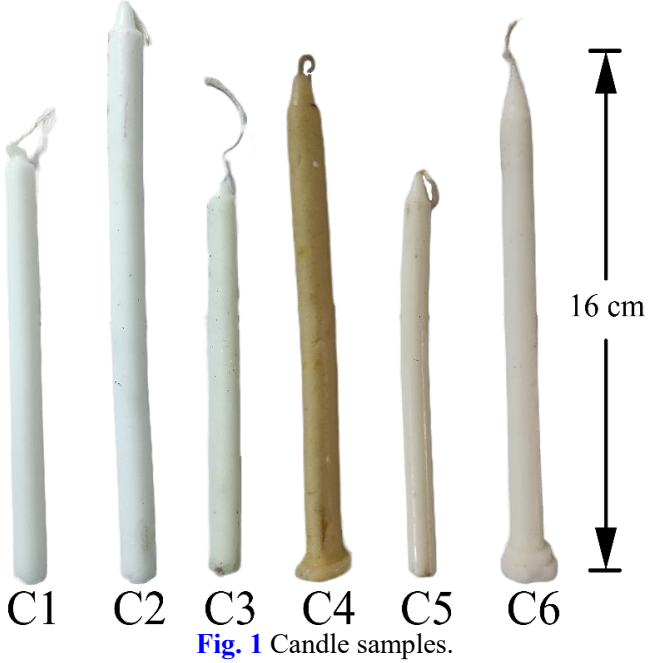

Fig. 1 Candle samples.

2.2 LIBS configuration

In the experiment, a Q-switched Nd: YAG laser (Q-smart 850) operating at 10Hz was employed with a second harmonic (wavelength 532nm) at a pulse energy of 190 mJ/pulse of diameter 5 mm focus through a biconvex lens of focal length 115 mm to initiate laser plasma in the candle flame. Laser per pulse energy density or fluence was 9.94×10^4 J/cm^2. The flash lamp Q-switch (FLQS) delay was changed to alter the pulse energy, and an energy meter (NOVA-QTL) was used to quantify it. Fiber optics were used to connect a spectrometer (HR4000, Ocean Optics) to collect the plasma emission, which has a wavelength range of 200-1100 nm. A remote LIBS setup consisting of a couple of plano-convex lenses of a focal length of 150 mm was used to travel light signal from laser produced plasma to optical fiber. The distance between the laser induced plasma to the first lens is 150 mm, and the distance between the second lens to the optical fiber of the spectrometer was also 150 mm, while the distance between these two lenses is 555 mm, aligned perpendicular to the laser beam. A delay generator (DG535, Stanford Research Systems) was used to adjust the timing of the triggering pulse for the Q-switch and spectrometer. As shown in Fig. 2, the delay time for the spectrometer to be triggered was set at 1 μs, and the integration time of the spectrometer was set at 50 ms so that the entire plasma emission could be accommodated. The standard deviation was calculated by averaging 30 spectra, which were repeated 100 times (3000 shots in total) at each measurement point. Two-dimensional (2-D) stage of traveling microscope with 0.1 mm least count for the precision movement was employed for spatial distribution assessment.

Fig. 3(a) shows a representative spectrum of the six flames used in this study without laser induced breakdown. We observed emission lines of K at wavelengths 766 nm and 769 nm, however, there are no H and O lines in the flame without laser induced breakdown. LIBS raw spectrum is represented in black color in Fig. 3(b). The Asymmetric Least Squares (AsLS) method was applied to remove the background emission by setting the baseline,[29] the defined baseline was subtracted from the raw spectrum, in the result the corrected spectrum represented as a red line in Fig. 3(b). The five spectra of candle flame at different vertical positions are presented in Fig. 3(c). Also, each spectrum was area normalized. Because of the transmission properties of the plano-convex lenses used to detect the remote LIBS signal, no spectra were observed below 300 nm. Blackbody radiation and plasma irradiation contribute to the raw spectrum's background emissions. Rayleigh scattering may be seen in the incident laser peak at 532 nm.

2.3 Classification methods

For unsupervised machine learning, the principal component analysis (PCA) method was used to distinguish between each of the six candle samples. Data dimension reduction with little information loss was achieved using PCA, a statistical approach.[30] There have been several approaches to employing supervised machine learning including decision trees, discriminant analysis, Naive Bayes, support vector machines (SVM), K nearest neighbors (KNN), ensemble, and Neural networks.

Decision trees for multiclass learning methods are simple to read, rapid, and need little memory, but may not be accurate enough. From the root to the final class, a tree structure guides decision-making (leaves). The tested variants are the Fine tree, Medium tree, and Coarse tree.[31]

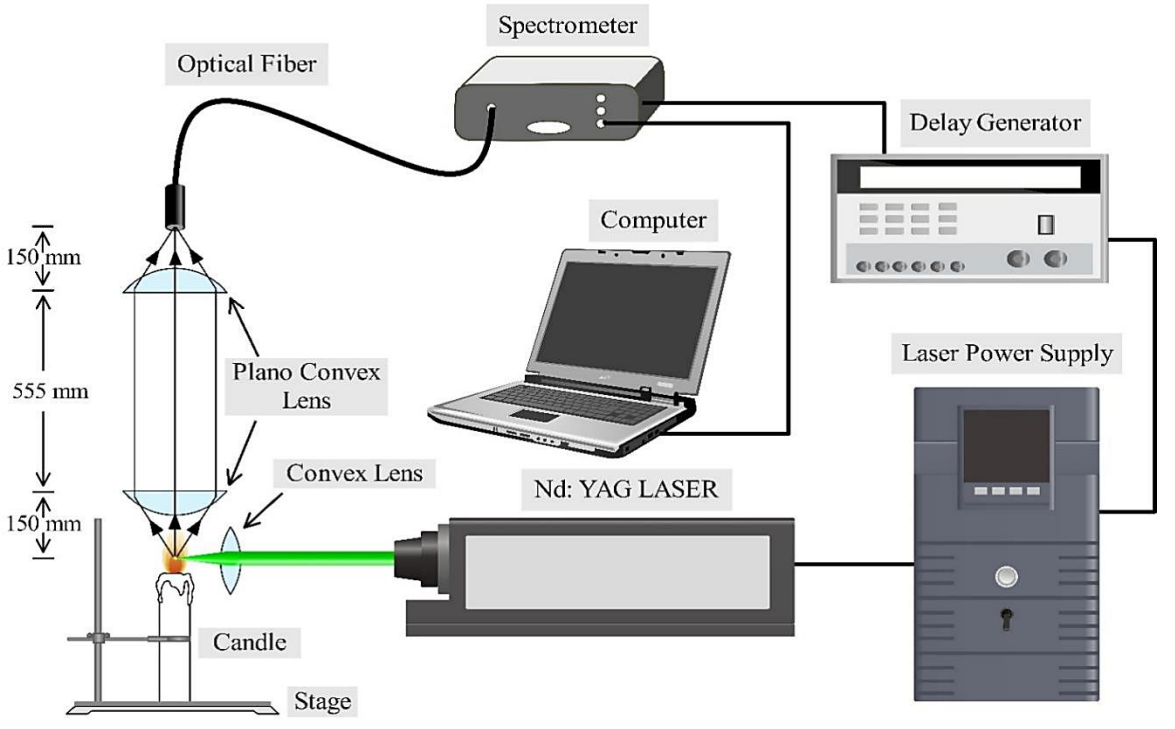

Fig. 2 LIBS experimental setup.

Regularized discriminant analysis (linear and quadratic) is simple to understand and quick for huge datasets. Using "Quadratic Discriminant" requires more RAM. It is a method of N-dimensional statistical analysis (multivariate statistical analysis) where items are grouped based on probability densities. Linear discriminant and Quadratic discriminant are examined.[32]

Gaussian, multinomial, or kernel predictor Naive Bayes model; this technique is simple to comprehend and produces good results for multi-class classification. Gaussian's

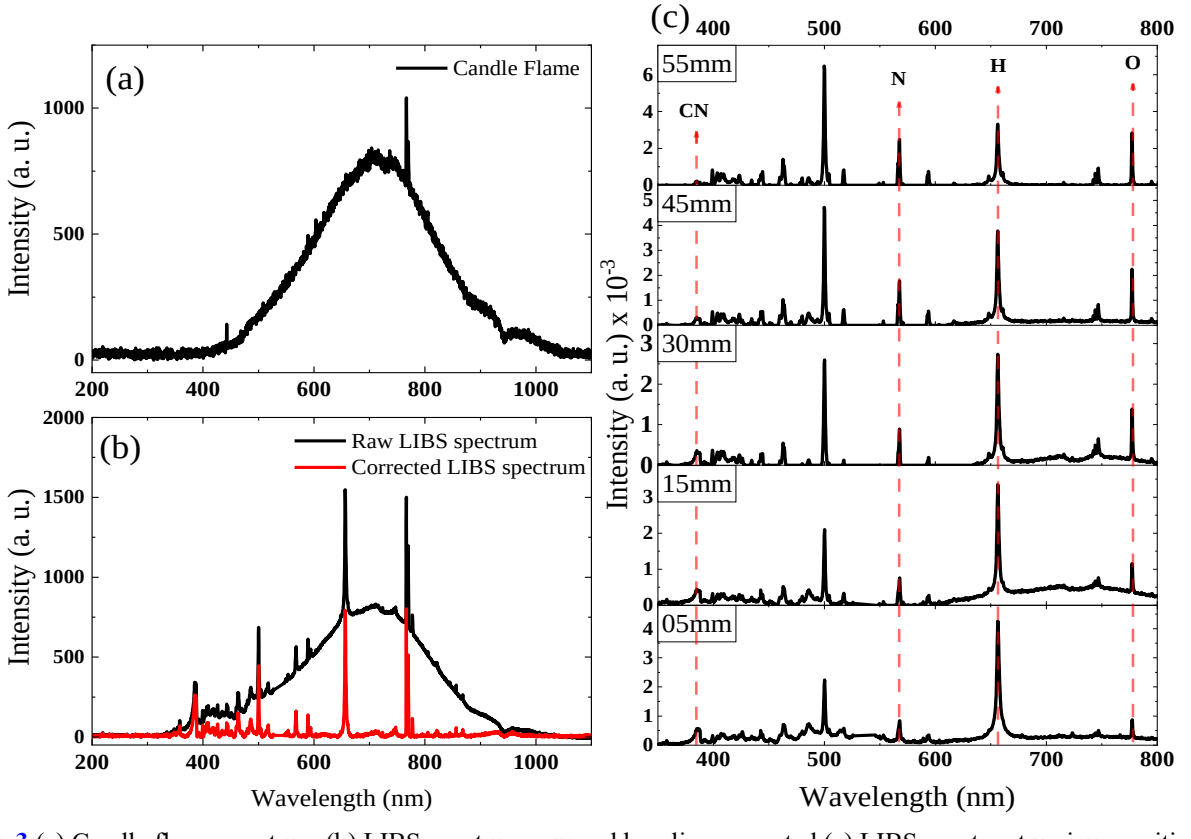

Fig. 3 (a) Candle flame spectrum (b) LIBS spectrum raw and baseline corrected (c) LIBS spectra at various positions.

prediction speed (medium) and memory consumption (medium) are both sluggish (small for Gaussian). Conditional probabilities and class affiliation tests are used in conjunction with Bayes' theorem. Thomas Bayes developed Bayes' Theorem in 1736, which is the classifier. Gaussian Naive Bayes and Kernel Naive Bayes are the two models that are being examined.[33]

It's tough to understand the results of binary or multiclass classification using SVM (not for the linear variant). Multi-class classification is slow because the issue must be broken into numerous partial binary problems, each requiring a significant amount of RAM. Using this approach, you may identify the boundaries between different classes of objects. In addition to Linear SVM, quadratic, cubic, and fine Gaussian SVM variations were investigated for their performance.[34]

Kd-tree search for K nearest neighbors (KNN) categorization. This is a challenging strategy to understand, and as the number of classes increases, so does its effectiveness. Speed and memory needs are the media for predicting. The method's core principle is to find objects in N-dimensional space that share the same characteristics as the class's nearest neighbors. The variants that have been put to the test are Fine KNN, Medium KNN, Coarse KNN, Cubic KNN, and Weighted KNN.[35]

Boosting, random forest, bagging, random subspace, and ECOC (Error-Correcting Output Codes) ensembles are some of the classification ensembles that may be used for multiclass learning. One strong model is created by combining multiple basic strategies. Despite this, the prediction speed is quick to medium (depending on the combination utilized) and memory consumption is modest (medium for Subspace KNN). These include Boosted Trees, RUSBoosted Trees, Bagged Trees, Subspace Discriminant, Subspace KNN, and Subspace KNN.[36]

A neural network is a set of algorithms that uses an approach similar to how the human brain works to attempt to find underlying correlations in a batch of data. In this framework, neural networks are systems of neurons that might be artificial or biological in origin. Because neural networks can adapt to changing input, they can deliver the best results possible without having to reevaluate the output criteria.[37]

Spectra were normalized by overall spectral intensity (*i.e.*, area of each spectrum) for supervised machine learning (each averaged over 30 spectra). Thus, the entire dataset (spectra with candle number labels) is divided into three datasets: one for training, one for validating the model, and one for testing. As a safeguard against overfitting, a 10-fold cross-validation approach was used to divide the data into folds and estimate the accuracy on each fold. The present experiments include two datasets: the training dataset, which contains all samples (candles) except 20%, and the prediction dataset, which contains the remaining 20%. The prediction dataset is not utilized for training or model validation, but merely for evaluating the model's performance on a random sample of the spectrum database.

3. Results and discussion

3.1 Burning rates

To distinguish among various candles, burning rates and flame structures were utilized conventionally. Candle burning rates were measured with time. Time in seconds on the x-axis vs mass in grams is shown in Fig. 4(a) for all six candles and the burning rate comparison in the histogram is presented in Fig. 4(b). A good linear relation can be seen in the burning rates of candles. Due to a significant difference in the mass burning rate of candles, it provides an attractive potential to distinguish between flames by utilizing the LIBS technique which can provide point information inside the flames, even for prediction of the local structure accurately by utilizing artificial intelligence.

3.2 H/O ratios

LIBS measurements were conducted in situ to measure the variable fuel to oxidizer ratio in the luminous diffusion flame of a candle. The spatial measurement location, vertically, starts from 5.0 mm from molten wax moving upward with the step size of 5.0 mm at the flame centerline, horizontally, starts on the center of the candle wick in the fuel-rich region then moves toward the edge of the flame with a step size of 0.5 mm. The LIBS spectra contain the hydrogen line H_α at 656 nm

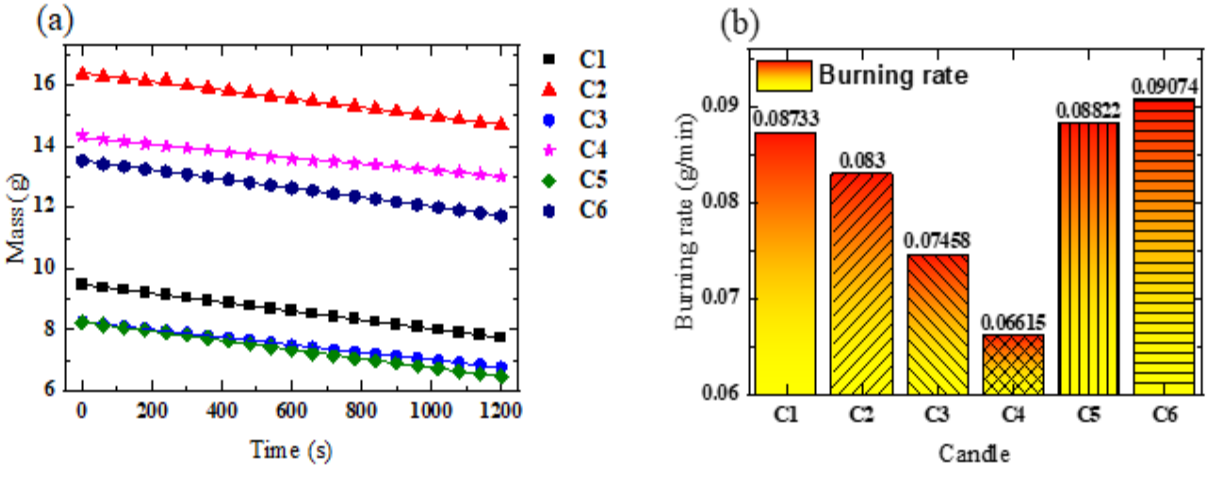

Fig. 4 (a) Burning rate and (b) mass consumption of candles.

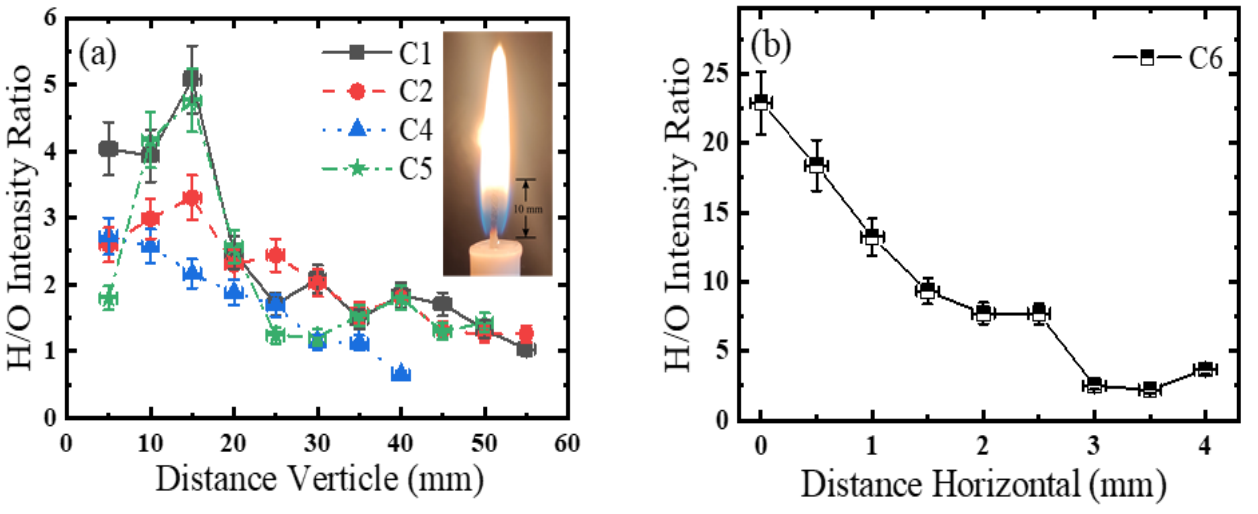

Fig. 5 (a) Vertical and (b) horizontal profile of H/O intensity ratio.

wavelength, oxygen O-I at 777 nm, nitrogen N-II at 567 nm, potassium K-I at 766 nm, and 769 nm. While molecular species, cyanogen (CN) band detected at 385 nm, CO at 451 nm, O_2 at 406 nm, CO_2 at 335 nm, and 375 nm were also observed.[38]

The H/O ratio was greatest near the flame's centerline and progressively dropped towards the flame's edge. This is because the concentrations of H and C near the flame centerline are high owing to the ionization/fragmentation of candle wax molecules. On the other hand, the concentration of O_2 molecules at the flame centerline is low in a diffusion kind of flame. Concentrations of O_2, CO_2, H_2O, and CO molecules, and hence of O atoms, rise as one approaches the flame's edge. However, when the fuel concentration decreases, the concentration of H atoms and hence the H/O ratio decreases, as seen by the vertical profile of H/O in Fig. 5(a), whereas Fig. 5(b) depicts the horizontal profile of the H/O intensity ratio. Individual emission line displays that fuel origin species H and CN emit stronger in the dark zone of a candle due to the fuel-rich region, while emission of oxidizer origin species N and O is stronger at the outer edges of a candle flame. In the luminous part of the candle, the flame continuum was observed as a result of that uplifted baseline found due to black body emission. In the fuel-rich area of a candle flame, soot particles should comprise volatile organic compounds (VOCs) and polycyclic aromatic hydrocarbons (PAHs). There is no need to worry about the material of the hollow's walls when it comes to radiation originating from a modest source in a cavity. At low temperatures, the hole in a cavity appears black, and the radiation emitted is known as black-body radiation or cavity radiation. The light of the sun is much like blackbody radiation. Soot particles could behave as a perfect black body in the candle flame, which absorb the energy of chemical reaction and emit a continuous spectrum. A significant decrease in laser-produced plasma was observed in the candle flame because of the absorption of plasma energy by soot particles.[39] H/O intensity ratio can be used as intrinsic propriety of LIBS in the flame for equivalence ratio determination.

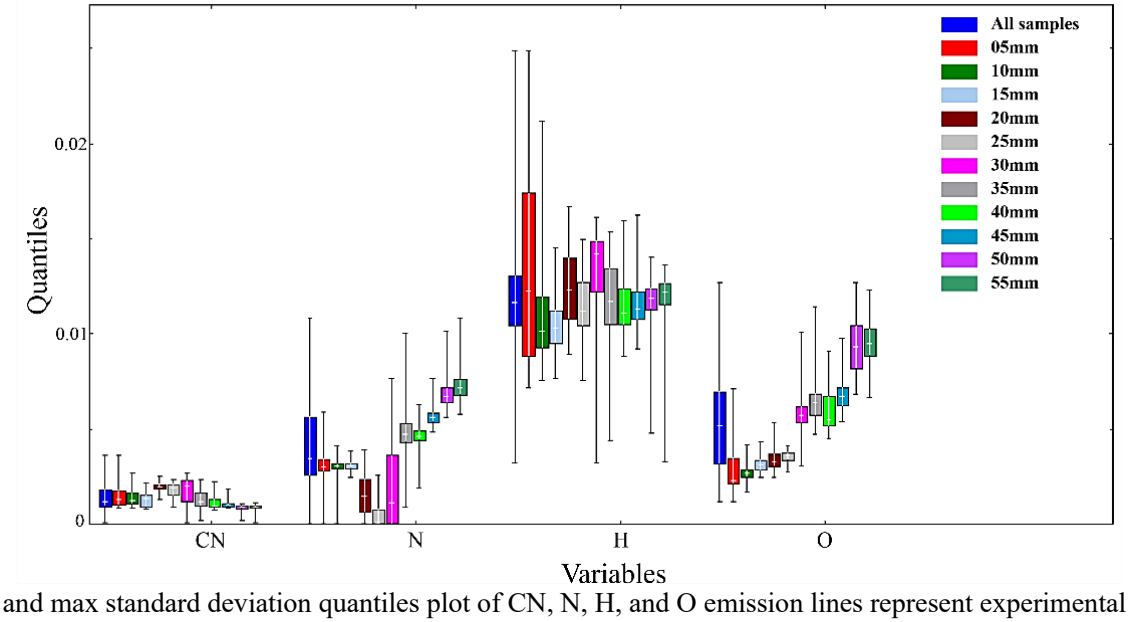

Fig. 6 Min and max standard deviation quantiles plot of CN, N, H, and O emission lines represent experimental uncertainty.

The experimental uncertainties occurred due to pulse-to-pulse fluctuation in laser energy, focused laser spot size, and the reflection of light from the lens. The output energy of a pulsed laser has a shot-to-shot fluctuation that results in uncertainties in the peak intensities of the LIBS spectrum. These uncertainties have been minimized by taking a very large number of spectra. The spectra used in this study resulted from 100 replicates each having an average of 30 spectra. This means that these 100 spectra contain data of 3000 laser shots. As a result, data could fluctuate because experimental uncertainties are present. Representative means elemental and molecular spectral intensities with min and max standard deviation quantiles plot of CN, N, H, and O shown in Fig. 6.

3.3 Comparison of classification results

Six candle flame spectra were subjected to PCA in order to distinguish between them and to show the distribution of the LIBS spectral data. It was determined that the first three main principal components (PCs) accounted for 91 percent of the variation in all spectra, with PC1 accounting for 54 percent, PC2 for 31 percent, and PC3 for 6 percent. A 2-D score plot of six candle flame samples was shown in Fig. 7 whereas a 3-D score plot of three PCs showed in Fig. 8 that PC1 was responsible for separating the data sets, confirming the apparent difference between the six data sets. Because of the PCs' and wavelengths' relativity, PCA loading is an important consideration. PCs that are heavily loaded exhibit the greatest range of results across all samples. As a result, PCA loading may be used to pick key emission lines whose wavelengths are associated.[40] As shown in Fig. 9, the loading plot for PCs 1, 2, and 3 reveals the variation in all wavelength variables. Eight PCs were utilized as feature selection by PCA component extraction with explained variance of 98 % (each component 55.0 %, 32.1 %, 5.9 %, 2.2%, 1.3%, 1.0 %, 0.4% and 0.3%). MATLAB Classification Learner App was used to implement classification models. 10 cross-validations of training data were used to fine-tune the parameters.

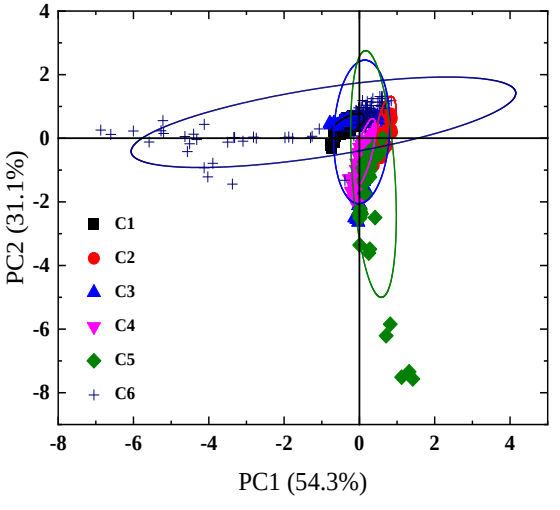

Fig. 7 The 2-D score plot of the first two principal components containing a cumulative 85.4% variance.

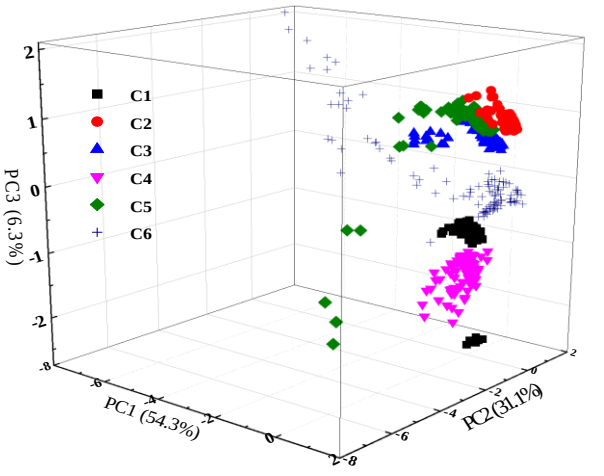

Fig. 8 The 3-D score plot of the first three principal components containing a cumulative 91.7% variance.

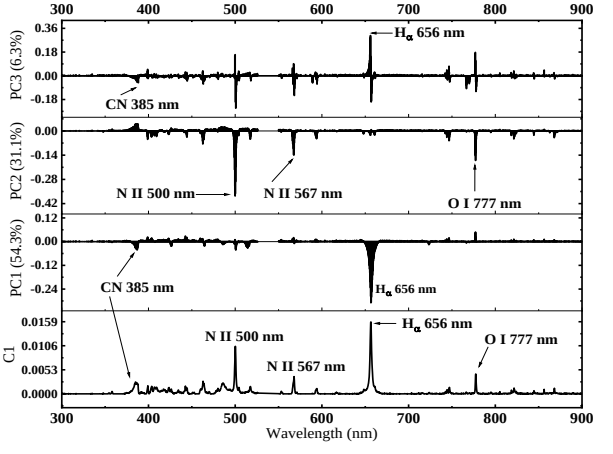

Fig. 9 Loading plots of candle flame samples.

Each model's accuracy is determined by the number of classifications a model accurately predicts divided by the total number of classifications produced by the model. Two instances were used to train, validate, and test the categorization models. Discrimination against candle flames has been performed in the first instance. In the second scenario, machine learning models predicted the vertical locations inside the candle flame at the centerline. Table 1 shows the classification results of candles (case 1: Distinguish between all Candles; case 2: Vertical position measurement of one representative sample C6) by comparing individual categorization models and their accuracies with the time each model spends on training.

In case 1: investigating several different types of classification models a majority of artificial intelligence models could provide accurate prediction with ≥ 95% efficiency. Further, it was found that the quadratic discriminant analysis (QDA) and Neural Network models provided the best option for training and class prediction. While linear SVM and quadratic SVM provides 99.8% training accuracy with 100% class prediction accuracy. A confusion matrix is a relation between true class versus predicted class, truly predicted values lie in the

diagonal of a matrix. The confusion matrix of the Wide Neural Network was produced from the trained model for distinguishing the six candles displayed in Fig. 10. Truly predicted classes are in the diagonal of the matrix. While false predicted entities lie outside of the diagonal of a matrix.

Table 1. Classification results of candles (case 1: Distinguish between all Candles; case 2: Vertical position measurement of one representative sample C6).

Classifier	Classifier Type	Case 1: Distinguish between all Candles			Case 2: Vertical position measurement of one representative sample C6		
		Training Accuracy (%)	Prediction Accuracy (%)	Time (sec)	Training Accuracy (%)	Prediction Accuracy (%)	Time (sec)
Decision Trees	Fine Tree	97.5	99.17	51	65.3	65.5	106
	Medium Tree	97.5	99.17	49	56.9	60.5	98
	Coarse Tree	78.5	77.5	71	39.2	42.7	135
Discriminant Analysis	Linear Discriminant	98.3	98.4	74	62	67.7	137
	Quadratic Discriminant	100	100	101	74.1	80.9	195
Naive Bayes	Gaussian Naive Bayes	97.3	94.17	102	55.9	60.5	192
	Kernal Naive Bayes	97.9	93.33	105	62	62.7	245
Support Vector Machines (SVM)	Linear SVM	99.8	100	136	74.7	74.1	253
	Quadratic SVM	99.8	100	169	84.5	85.5	312
	Cubic SVM	99.8	99.17	165	84.8	86.4	319
	Fine Gaussian SVM	97.3	97.5	193	58.1	64.1	369
	Medium Gaussian SVM	68.3	74.17	196	42.8	44.5	377
	Coarse Gaussian SVM	66.9	73.33	226	41.9	45	460
K Nearest Neighbor (KNN)	Fine KNN	99.4	99.17	225	73.3	74.1	456
	Medium KNN	98.5	98.33	256	69.4	72.7	490
	Coarse KNN	84.8	96.67	253	51	57.7	515
	Cosine KNN	99.4	100	280	68.2	71.4	634
	Cubic KNN	98.3	98.33	284	69.9	74.1	671
	Weighted KNN	99.0	99.17	306	73.1	77.7	671
Ensemble Classifiers	Boosted Trees	16.7	16.67	312	63.3	64.5	834
	Bagged Tree	98.8	99.17	345	73.1	74.5	892
	Subspace Discriminant	97.9	97.5	349	61.1	67.7	877
	Subspace KNN	98.5	100	383	70.1	77.3	912
	RUS Boosted Trees	16.7	16.67	375	56.9	60.5	954
Neural Network	Narrow Neural Network	99.4	99.2	401	85	84.1	979
	Medium Neural Network	99.8	100	406	84.2	82.1	1025
	Wide Neural Network	99.6	100	424	86	76.8	1039
	Bilayered Neural Network	100	100	430	84	80	1097
	Trilayered Neural Network	98.8	99.2	442	82.8	75	1109

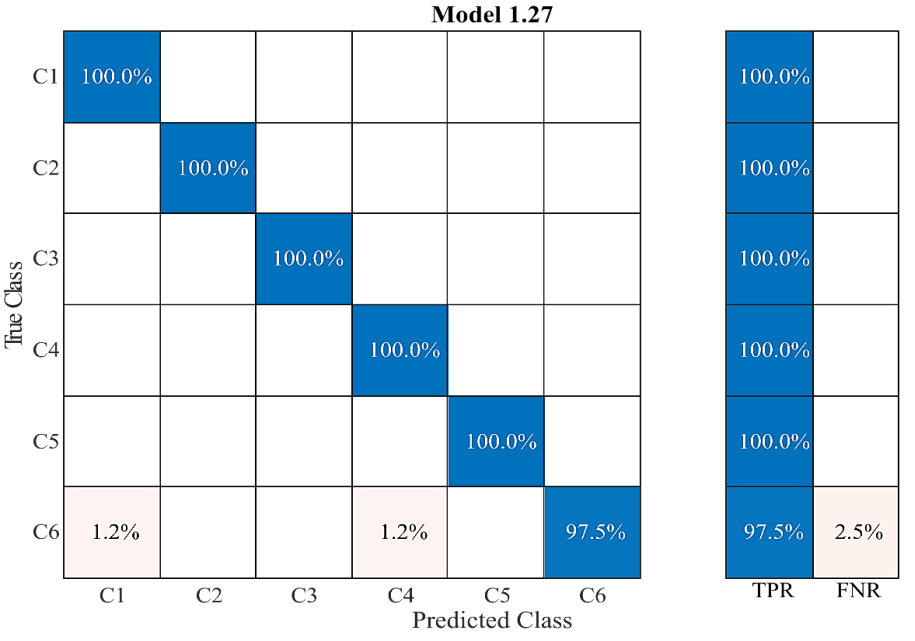

Fig. 10 Confusion matrix of Wide Neural Network for distinguishing six candles.

In case 2: while getting the vertical local prediction of position inside the candle flame, most of the classification models provide accuracies in the range of 60% to 85%. The accuracies of classification models are slightly less as compared to case one because the outliers lie in the spectral data due to the trembling of the candle's flame with the shockwave of laser-produced plasma. The cubic SVM, quadratic SVM, and Neural Network models provided the best option for training and class prediction. The confusion matrix of Wide Neural Network for vertical position measurement of candle No. C6 is presented in Fig. 11. The position was predicted well inside the candle flame. Truly predicted classes are in the diagonals of the matrix. While false prediction lies outside of the matrix that is mostly one step above or below that particular position because of the trembling of flame.

Overall, for the training of models with limited resources of computation Decision Trees and Discriminant Analysis models are a good choice but for the medium computation resources, SVM and KNN are preferable. Ensemble and Neural Network models consume great resources of computation. Neural Network models give state-of-the-art classification accuracy for both cases distinguishing between all candles and vertical position measurements.

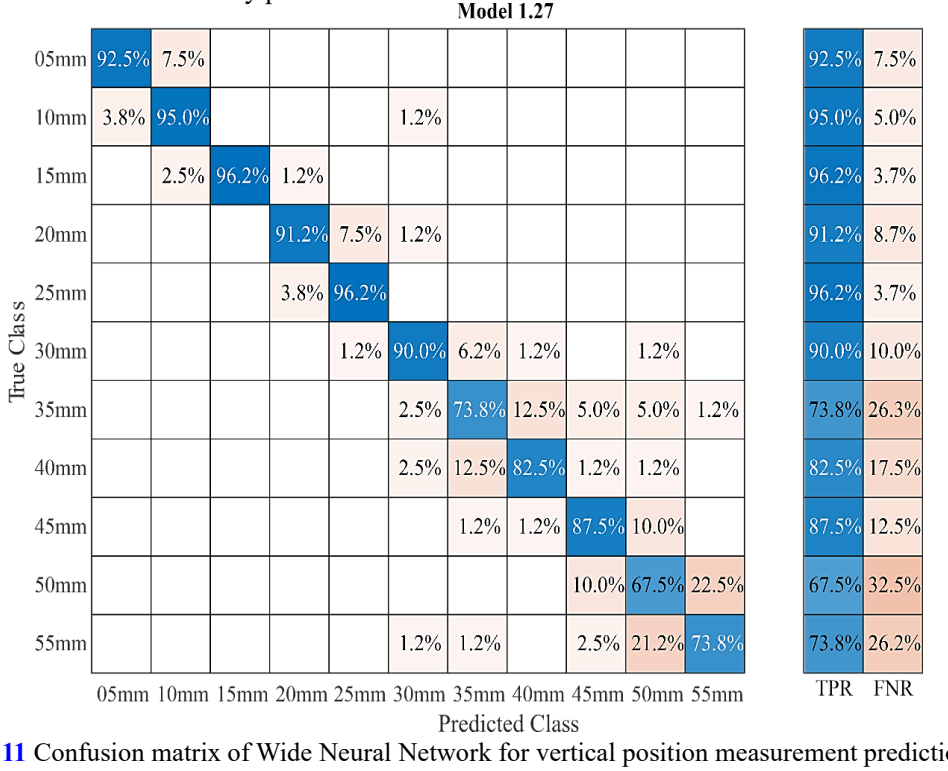

Fig. 11 Confusion matrix of Wide Neural Network for vertical position measurement prediction.

5. Conclusions

LIBS was used to describe the local structures of certain diffusion flames to discriminate among candle flames using machine learning. The H/O ratios were high at the flame centerline and gradually decreased moving toward the border of flame, which is because at the flame centerline the concentrations of H and C are high due to the ionization/fragmentation of candle wax molecules. The implementation of PCA on LIBS data was unable to provide sufficient discrimination among all six candles. Further, the implementation of supervised machine learning classification models has shown unprecedented differentiability. For case one, the QDA and Neural Network models provided the best results for training and class prediction. While linear SVM, quadratic SVM, fine KNN, Cosine KNN, and Neural networks provided more than 99% training and prediction accuracy. For case two, the cubic SVM, quadratic SVM, and Neural Network models provided the best option for training and class prediction. Such studies, based on artificial intelligence, and other flames such as jet flames, can further enhance the efficiency of jet engines.

Acknowledgments

The authors are grateful for the financial support from the the National Science and Technology Major Project (J2019-III-0005-0048), MOST (2021YFA0716200), Natural Science Foundation of China (No. 52161145105/51976216), Beijing Municipal Natural Science Foundation (JQ20017) and K.C. Wong Education Foundation (GJTD-2020-07).

Conflict of Interest

The authors declare no conflict of interest.

Supporting Information

Not applicable.

References

[1] F. Liu, K. A. Thomson, G. J. Smallwood, Effects of soot absorption and scattering on LII intensities in laminar coflow diffusion flames, *Journal of Quantitative Spectroscopy and Radiative Transfer*, 2008, **109**, 337-348, doi: 10.1016/j.jqsrt.2007.08.027.

[2] C. Liu, L. Xu, Z. Cao, H. McCann, Reconstruction of axisymmetric temperature and gas concentration distributions by combining fan-beam TDLAS with onion-peeling deconvolution, *IEEE Transactions on Instrumentation and Measurement*, 2014, **63**, 3067-3075, doi: 10.1109/tim.2014.2315737.

[3] Y. Du, Z. Peng, Y. Ding, High-accuracy sinewave-scanned direct absorption spectroscopy, *Optics Express*, 2018, **26**, 29550, doi: 10.1364/oe.26.029550.

[4] Q.-X. Huang, F. Wang, D. Liu, Z.-Y. Ma, J.-H. Yan, Y. Chi, K.-F. Cen, Reconstruction of soot temperature and volume fraction profiles of an asymmetric flame using stereoscopic tomography, *Combustion and Flame*, 2009, **156**, 565-573, doi: 10.1016/j.combustflame.2009.01.001.

[5] D. R. Snelling, K. A. Thomson, G. J. Smallwood, O. L. Gulder, E. J. Weckman, R. A. Fraser, Spectrally resolved measurement of flame radiation to determine soot temperature and concentration, *AIAA Journal*, 2002, **40**, 1789-1795, doi: 10.2514/3.15261.

[6] J. Ballester, T. García-Armingol, Diagnostic techniques for the monitoring and control of practical flames, *Progress in Energy and Combustion Science*, 2010, **36**, 375-411, doi: 10.1016/j.pecs.2009.11.005.

[7] A. Iftikhar, Y. Jamil, N. Nazeer, M. S. Tahir, N. Amin, Optical emission spectroscopy of nickel-substituted cobalt-zinc ferrite, *Journal of Superconductivity and Novel Magnetism*, 2021, **34**, 1849-1854, doi: 10.1007/s10948-020-05734-5.

[8] M. Pardede, T. J. Lie, J. Iqbal, M. Bilal, R. Hedwig, M. Ramli, A. Khumaeni, W. S. Budi, N. Idris, S. N. Abdulmadjid, A. M. Marpaung, I. Karnadi, I. Tanra, Z. S. Lie, H. Suyanto, D. P. Kurniawan, K. H. Kurniawan, K. Kagawa, M. O. Tjia, H-D analysis employing energy transfer from metastable excited-state He in double-pulse LIBS with low-pressure He gas, *Analytical Chemistry*, 2019, **91**, 1571-1577, doi: 10.1021/acs.analchem.8b04834.

[9] M. Pardede, I. Karnadi, R. Hedwig, I. Tanra, J. Iqbal, M. Alion Marpaung, M. Margaretha Suliyanti, E. Jobiliong, S. Nur Abdulmadjid, N. Idris, A. Khumaeni, M. Shiddiq, M. Gracio A. Rhizma, Z. Sukra Lie, M. Bilal, D. Putra Kurniawan, T. Jie Lie, K. Hendrik Kurniawan and K. Kagawa, High sensitivity hydrogen analysis in zircaloy-4 using helium-assisted excitation laser-induced breakdown spectroscopy, *Scientific Reports*, 2021, **11**, 21999, doi: 10.1038/s41598-021-01601-y.

[10] K. E. Eseller, F. Y. Yueh, J. P. Singh, Laser-induced breakdown spectroscopy measurement in methane and biodiesel flames using an ungated detector, *Applied Optics*, 2008, **47**, G144, doi: 10.1364/ao.47.00g144.

[11] M. Gragston, P. Hsu, N. Jiang, S. Roy, Z. Zhang, Emissions in short-gated ns/ps/fs-LIBS for fuel-to-air ratio measurements in methane-air flames, *Applied Optics*, 2021, **60**, C114, doi: 10.1364/ao.418453.

[12] M. Gragston, P. Hsu, A. Patnaik, Z. Zhang, S. Roy, Time-gated single-shot picosecond laser-induced breakdown spectroscopy (ps-LIBS) for equivalence-ratio measurements, *Applied Spectroscopy*, 2020, **74**, 340-346, doi: 10.1177/0003702819885647.

[13] L.-J. Hsu, Z. T. Alwahabi, G. J. Nathan, Y. Li, Z. S. Li, M. Aldén, Sodium and potassium released from burning particles of brown coal and pine wood in a laminar premixed methane flame using quantitative laser-induced breakdown spectroscopy, *Applied Spectroscopy*, 2011, **65**, 684-691, doi: 10.1366/10-06108.

[14] M. Kotzagianni, E. Kakkava, S. Couris, Laser-induced breakdown spectroscopy (LIBS) for the measurement of spatial structures and fuel distribution in flames, *Applied Spectroscopy*, 2016, **70**, 627-634, doi: 10.1177/0003702816631296.

[15] Y. Lan, Y. Lu, X. Dong, R. Zheng, Detection improvement of laser-induced breakdown spectroscopy using the flame generated from alcohol-solution mixtures, *Optics Express*, 2019, **27**, 29896, doi: 10.1364/oe.27.029896.

[16] L. Liu, S. Li, X. N. He, X. Huang, C. F. Zhang, L. S. Fan, M.

X. Wang, Y. S. Zhou, K. Chen, L. Jiang, J. F. Silvain, Y. F. Lu, Flame-enhanced laser-induced breakdown spectroscopy, *Optics Express*, 2014, **22**, 7686, doi: 10.1364/oe.22.007686.
[17] A. E. Majd, A. S. Arabanian, R. Massudi, M. Nazeri, Spatially resolved laser-induced breakdown spectroscopy in methane—air diffusion flames, *Applied Spectroscopy*, 2011, **65**, 36-42, doi: 10.1366/10-05863.
[18] B. Tai, X. Hao, J. Wang, H. Sun, Flame temperature measurement based on laser-induced breakdown spectroscopy and element doping, *ACS Omega*, 2021, **6**, 27239-27246, doi: 10.1021/acsomega.1c04025.
[19] R. Wu, J. Wei, B. Zhang, J. Li, X. Song, W. Su, F. Xie, P. Lv, G. Yu, In situ diagnostic investigation on the structure distribution of inverse diffusion flames based on laser-induced breakdown spectroscopy, *Fuel*, 2022, **311**, 122540, doi: 10.1016/j.fuel.2021.122540.
[20] H. Zhang, K. Hippalgaonkar, T. Buonassisi, O. M. Løvvik, E. Sagvolden, D. Ding, Machine Learning for Novel Thermal-Materials Discovery: Early Successes, Opportunities, and Challenges, arXiv preprint arXiv:1901.05801, 2019, 1-16, doi: 10.48550/arXiv.1901.05801
[21] Z. He, M. Yang, L. Wang, E. Bao, H. Zhang, Concentrated Photovoltaic Thermoelectric Hybrid System: An Experimental and Machine Learning Study, *Engineered Science*, 2021, **15**, 47-56, doi: 10.30919/es8d440
[22] Z. Zheng, X. Lin, M. Yang, Z. He, E. Bao, H. Zhang, Z. Tian, Progress in the Application of Machine Learning in Combustion Studies, *ES Energy & Environment*, 2020, **9**, 1-14, doi: 10.30919/esee8c795
[23] K. Wan, S. Hartl, L. Vervisch, P. Domingo, R. S. Barlow, C. Hasse, Combustion regime identification from machine learning trained by Raman/Rayleigh line measurements, Combustion and Flame, 2020, **219**, 268-274, doi: 10.1016/j.combustflame.2020.05.024.
[24] Z. Zhou, Y. Ge, Y. Liu, Real-time monitoring of carbon concentration using laser-induced breakdown spectroscopy and machine learning, *Optics Express*, 2021, **29**, 39811-39823, doi: 10.1364/oe.443732.
[25] G. Teng, Q. Wang, X. Cui, G. Chen, K. Wei, X. Xu, B. S. Idrees, M. Nouman Khan, Predictive data clustering of laser-induced breakdown spectroscopy for brain tumor analysis, *Biomedical Optics Express*, 2021, **12**, 4438, doi: 10.1364/boe.431356.
[26] D. Sun, Design of time-delayed safety switches for CRISPR gene therapy, *Scientific Reports*, 2021, **11**, 16908, doi: 10.1038/s41598-021-96510-5.
[27] J. Moros, J. Serrano, F. J. Gallego, J. Macías, J. J. Laserna, Recognition of explosives fingerprints on objects for courier services using machine learning methods and laser-induced breakdown spectroscopy, *Talanta*, 2013, **110**, 108-117, doi: 10.1016/j.talanta.2013.02.026.
[28] J. Lee, B. McGann, S. D. Hammack, C. Carter, T. Lee, H. Do, M. S. Bak, Machine learning based quantification of fuel-air equivalence ratio and pressure from laser-induced plasma spectroscopy, *Optics Express*, 2021, **29**, 17902, doi: 10.1364/oe.425096.
[29] J. Korkisch, I. Steffan, M. B. Fisk, Chemical analysis of Manganese nodules, *Analytica Chimica Acta*, 1979, **108**, 63-68, doi: 10.1016/s0003-2670(01)93040-5.
[30] Y. Zhangcheng, Y. Liu, S. Saleem, Q. Zhang, Y. Chen, Y. Qu, X. Lu, Online in situ detection and rapid distinguishing of saffron, *Journal of Laser Applications*, 2020, **32**, 032020, doi: 10.2351/7.0000137.
[31] S. Moncayo, S. Manzoor, F. Navarro-Villoslada, J. O. Caceres, Evaluation of supervised chemometric methods for sample classification by Laser Induced Breakdown Spectroscopy, *Chemometrics and Intelligent Laboratory Systems*, 2015, **146**, 354-364, doi: 10.1016/j.chemolab.2015.06.004.
[32] G. Baudat, F. Anouar, Generalized discriminant analysis using a kernel approach, *Neural Computation*, 2000, **12**, 2385-2404, doi: 10.1162/089976600300014980.
[33] D. D. Lewis, in European conference on machine learning, Springer, 1998, 4-15.
[34] N. Cristianini, J. Shawe-Taylor, An Introduction to Support Vector Machines and Other Kernel-based Learning Methods. Cambridge: *Cambridge University Press*, 2000, doi: 10.1017/cbo9780511801389.
[35] K. Fukunaga, P. M. Narendra, A branch and bound algorithm for computing k-nearest neighbors, *IEEE Transactions on Computers*, 1975, **100**, 750-753, doi: 10.1109/t-c.1975.224297.
[36] T. G. Dietterich, Ensemble methods in machine learning. *Cagliari, Italy: Proceedings of the 1st International Workshop on Multiple Classifier Systems*, 2000: 1-15, doi: 10.1007/3-540-45014-9_1.
[37] X. Wang, X. Lin, X. Dang, Supervised learning in spiking neural networks: a review of algorithms and evaluations, *Neural Networks*, 2020, **125**, 258-280, doi: 10.1016/j.neunet.2020.02.011.
[38] M. I. Khan, N. U. Rehman, S. Khan, N. Ullah, Asad Masood, Aman Ullah, Spectroscopic study of CO_2 and CO_2–N_2 mixture plasma using dielectric barrier discharge, *AIP Advances*, 2019, **9**, 85015-85023, doi: 10.1063/1.5096399.
[39] M. Derudi, S. Gelosa, A. Sliepcevich, A. Cattaneo, D. Cavallo, R. Rota, G. Nano, Emission of air pollutants from burning candles with different composition in indoor environments, *Environmental Science and Pollution Research*, 2014, **21**, 4320-4330, doi: 10.1007/s11356-013-2394-2.
[40] X. Liu, X. Feng, F. Liu, J. Peng, Y. He, Rapid identification of genetically modified maize using laser-induced breakdown spectroscopy, *Food and Bioprocess Technology*, 2019, **12**, 347-357, doi: 10.1007/s11947-018-2216-0.

Author Information

Muhammad Bilal *received his Master degree in 2017 from the Department of Physics, University of Agriculture Faisalabad, Pakistan. He is pursuing his PhD in engineering thermophysics at the Institute of Engineering Thermophysics, University of*

Chinese Academy of Sciences. He is working under the supervision of Prof. Zhen-Yu Tian. His main areas of research interest are laser diagnostics of combustion and microgravity combustion.

Dr. Yasir Jamil *got his PhD at the Quaid I Azam University, Islamabad, Pakistan in 2009. From December 2013, he works as Associate Professor at the Department of Physics, University of Agriculture Faisalabad, Pakistan. Jamil's group mainly focuses on the Laser matter interaction, various applications of Lasers like agriculture, nanomaterials, energy and environment. The current project is spectrochemical analysis of pollutants in soil and vegetation using laser induced breakdown spectroscopy.*

Prof. Zhen-Yu Tian *got his PhD at the University of Science and Technology in 2008. Then he did a postdoc at CNRS in France (2008-2010) and worked at Bielefeld University as an Alexander von Humboldt Fellow and group leader (2010-2013). From August 2013, he works as a full Professor at the Institute of Engineering Thermophysics, Chinese Academy of Sciences (CAS). Tian's group mainly focuses on the combustion kinetics of engines, thin films, catalysis, environmental chemistry, microgravity combustion and physical chemistry. The current project is the kinetic study of homogeneous and heterogeneous combustion.*